

Promising Properties of Sub-5 nm Monolayer MoSi₂N₄ Transistor

Junsheng Huang¹, Ping Li¹, Xiaoxiong Ren¹ and Zhi-Xin Guo^{1,2,3*}

1. State Key Laboratory for Mechanical Behavior of Materials, Center for Spintronics and Quantum System, School of Materials Science and Engineering, Xi'an Jiaotong University, Xi'an, Shaanxi, 710049, China.

2. Key Laboratory of Polar Materials and Devices, Ministry of Education.

3. Department of Physics and Institute for Nanophysics, Xiangtan University, Xiangtan 411105, China

* E-mail: zxguo08@xjtu.edu.cn

Keywords: MoSi₂N₄, 2D FETs, electronic properties, ab initio quantum transport simulations, performance limit

Abstract

Two-dimensional (2D) semiconductors have attracted tremendous interests as natural passivation and atomically thin channels that could facilitate continued transistor scaling. However, air-stable 2D semiconductors with high performance were quite elusive. Recently, extremely air-stable MoSi₂N₄ monolayer had been successfully fabricated [Hong *et al.*, Science 369, 670 (2020)]. To further reveal its potential applications in the sub-5 nm MOSFETs, there is an urgent need to develop integrated circuits. Here we report first-principles quantum transport simulations on the performance limits of n- and p-type sub-5 nm monolayer (ML) MoSi₂N₄ metal-oxide-semiconductor FETs (MOSFETs). We find that the on-state current in the MoSi₂N₄ MOSFETs can be effectively manipulated by the length of gate and underlap (UL), as well as the doping concentration. Very strikingly, we also find that the n-type devices the optimized on-state current can reach up to 1390 and 1025 $\mu\text{A}/\mu\text{m}$ for the

high performance (HP) and low power (LP) applications, respectively, both of which satisfy the International Technology Roadmap for Semiconductors (ITRS) requirements. Whereas, the optimized on-state current can meet the LP application ($348 \mu\text{A}/\mu\text{m}$) for the p-type devices. Finally, we find that the MoSi_2N_4 MOSFETs have ultra-low subthreshold swing and power delay product, which have potential to realize the high speed and low power consumption devices. Our results show that MoSi_2N_4 is an ideal 2D channel material for future competitive ultrascaled devices.

I. INTRODUCTION

The downscaling of field-effect transistors (FETs) to the sub-7 nm channel length is in great demand for integrated circuits in the next decade. [1,2] However, traditional silicon FETs are suffering from the challenges of the short-channel effect, increased leakage current, and unnecessary power consumption. [3–5] To better solve these problems, numerous researchers have focused their attention on two-dimensional (2D) materials. Compared with that of three-dimensional materials, the uniform thickness and smooth surfaces of 2D materials are beneficial for high-speed application due to their suppressed carrier scattering and possible trap generation. Moreover, the atomically thin thickness of 2D materials make them ideal gate electrostatics with diminished short-channel effects and leakage currents. [6–14]

To date, layered transition-metal dichalcogenides (TMDCs) such as MoS_2 are the mostly studied 2D semiconductor material in FETs. [15–19] For example, the bilayer MoS_2 transistor with a 1 nm carbon nanotube (CNT) gate had been experimentally fabricated and found to exhibit an excellent gate control ability with subthreshold

swing (SS) of ~ 65 mV/dec and a remarkable on/off current ratio of 10^6 . [15] However, the on-state current ($< 250 \mu\text{A } \mu\text{m}^{-1}$) of the 2D MoS_2 FETs is too low to meet ITRS [20] standard for both HP and LP applications, [15–19] owing to the small carrier mobility of MoS_2 . On the other hand, some 2D materials such as 2D InSe and black phosphorene (BP) have much higher carrier mobility and excellent performance with high on-currents, which can satisfy the ITRS requirements for both HP and LP standards with the device scaled down to ~ 5 nm. [21–23] However, their instability in air is an issue, which greatly limits the device fabrications and applications. [21,23] Although numerous efforts have been devoted to explore new 2D materials, such as silicene, tellurene, $\text{Bi}_2\text{O}_2\text{Se}$, WSe_2 , GeSe , ReS_2 , BiN , AsP , [24–33] for the sub-5 nm FETs, the 2D material with both excellent device performance and air-environmentally stability is still scarce.

Recently, a new 2D material MoSi_2N_4 has been successfully synthesized by chemical vapor deposition (CVD). [34] This material is excellent ambient stability, e.g. it can be stable even in immersion in HCl aqueous solution for 24 hours. [34] MoSi_2N_4 is also a semiconductor, the band gap of which can be efficiently tuned by either strain or electric field. [35–37] In combination with the characteristics of highly controllable growth and good ohmic contact with electrodes, such as Ti, Sc, Ni and NbS_2 , MoSi_2N_4 has great potential applications in the next-generation FET devices. [34,38,39]

Here we theoretically investigate the performance of n- and p-type sub-5 nm double-gated (DG) ML MoSi_2N_4 MOSFETs by using *ab initio* quantum transport

calculations. We find that the transmission channel of ML MoSi₂N₄ locates in the MoN₂ layer sandwiched between two Si-N layers [as indicated in Fig. 1]. The main critical device properties, including the on-state current (I_{on}), SS, delay time (τ) and power-delay product (PDP), have been taken into consideration. More importantly, we also find that the on-state current of the optimized n-type ML MoSi₂N₄ MOSFET for HP is as high as 1390 $\mu\text{A}/\mu\text{m}$. The n-type ML MoSi₂N₄ MOSFET can meet the ITRS standards for HP and LP devices when scaled down to 3 nm and 1 nm, respectively. Whereas, the p-type ML MoSi₂N₄ MOSFET can only satisfy the ITRS LP requirement when it scaled down to 3 nm. Moreover, we find that the MoSi₂N₄ MOSFET has excellent gate controllability with a quite small SS, and its delay time and PDP are small enough to meet the ITRS HP and LP requirements.

II. METHOD

The geometric optimization and electronic structures of monolayer MoSi₂N₄ were calculated by density-functional theory (DFT) with the projector augmented wave (PAW) method, which is implemented in the Vienna *ab initio* simulation package (VASP). [40–42] The exchange-correlation function was described based on the generalized gradient approximation (GGA) in the form of Perdew-Burke-Ernzerhof (PBE) parameterization. [43] The convergence standards of the atomic energy and positions are less-than 1×10^{-6} eV per atom and 1×10^{-2} eV \AA^{-1} , respectively. The cutoff energy of the wave function was set to 500 eV. The Brillouin zone was sampled by $15 \times 15 \times 1$ Monkhorst-Pack k-point mesh [44] for geometrical optimization and $21 \times 21 \times 1$ for electronic states.

The transport properties were simulated based on the DFT method combined with the nonequilibrium Green's function (NEGF) formalism, using the Atomistix ToolKit (ATK) 2019 package. [45,46] The drain current at a given bias voltage V_b and gate voltage V_g was calculated through the Landauer-Büttiker formula: [47]

$$I(V_g, V_b) = \frac{2e}{h} \int_{-\infty}^{+\infty} \{T(E, V_b, V_g)[f_s(E - \mu_s) - f_d(E - \mu_d)]\} dE \quad (1)$$

where $T(E, V_b, V_g)$ is the transmission coefficient, f_s and f_d stands for the Fermi-Dirac distribution functions for the source and drain, respectively. μ_s and μ_d stands for the electrochemical potentials of the source and drain, respectively. In the calculations, the Tier 3 basis set was adopted with HGH pseudopotentials, and generalized gradient approximation (GGA) in the form of PBE function was utilized to represent the exchange and correlation interactions. Because of the heavily screened electron-electron interaction by doping carriers, DFT GGA-based single-electron approximation is good in the description of the device electronic structure. [22,48,49] The real-space mesh cutoff was chosen to be 75 hartree, and the k-point meshes [44] were set as Monkhorst-Pack $11 \times 1 \times 129$ and $11 \times 1 \times 1$ for the electrode region and the central region in the Brillouin zone. Moreover, the boundary condition along the transverse, vertical, and transport directions were set to be periodic, Neumann, and Dirichlet type, respectively. [50]

III. RESULT AND DISCUSSION

A. Channel materials and device configuration

The atomic structure of ML MoSi_2N_4 is shown in Fig. 1(a), which can be regarded as a MoN_2 layer sandwiched between two Si-N layers [44]. The optimized lattice parameter of ML MoSi_2N_4 is 2.91 Å, in good agreement with previous

results. [34] The band-decomposed charge-density distributions [Fig. 1(b)] on valence-band maximum (VBM) and conduction-band minimum (CBM) show that the CBM and VBM of monolayer MoSi_2N_4 are mainly contributed by the middle MoN_2 layer. Fig. 1(c) further shows that the valence and conduction bands of ML MoSi_2N_4 are mainly contributed by d_z^2 and $d_{x^2-y^2}$ orbitals of Mo atoms, and Si and N atoms contribute little to them [Fig. S1 within the Supplemental Material [51]]. This feature means that the middle MoN_2 layer would be responsible for the electron transmission, which is verified by the transmission eigenstates calculations as shown in Fig. 1(d). Since the transmission pathway in MoN_2 is protected by the two outside Si-N bilayers, the MoSi_2N_4 can be recognized as a natural micro-wire with conduction wire surrounded by insulator wire.

The performance of MoSi_2N_4 MOSFETs was further investigated in use of ATK package. In the simulation, double gates were adopted, and degenerately doped ML MoSi_2N_4 was selected as two-probe electrodes [Fig. 2(a)]. Compared with the single gate case, dual gates can obviously increase the competence of gate modulation. [52] The electron transport direction is along the zigzag direction of MoSi_2N_4 , and the gate was assumed to be an ideal rectangle in the device model. In the calculation, the electrodes with length of about 1 nm was adopted and the dielectric constant of silicon dioxide was set to be 3.9. As indicated in Fig. 2(a), in the channel the gate region is usually shorter than the dielectric region, and the uncovered dielectric region is called underlap region. Previous studies found that the gate underlap, which is the spacer area between the gate and electrode, plays an essential role in the scalability of gate

length for the modeled FETs. [22] The proper length of the gate underlap, L_{UL} , could improve the device performance. Thus one can define the channel length (L_{ch}) as the sum of the gate length (L_g) and twice the length of the underlap (L_{UL}), namely, $L_{ch} = L_g + 2L_{UL}$. In the calculation, the atomic compensation charges method was used for doping in the electrodes and the doping concentration of $1.0 \times 10^{13} \text{ cm}^{-2}$ was adopted, unless otherwise specified. According to the ITRS 2013 edition requirements for HP and LP standards of sub-5 nm device in 2028, we used 0.64 V as the supply voltage (V_{dd}) and 0.41 nm as the equivalent oxide thickness (EOT) of dielectric material (silicon dioxide). Various length of the gate underlap ranging from 0-4 nm was considered for a comprehensive investigation on the performance of MoSi₂N₄ MOSFETs.

B. On-state current

On-state current (I_{on}) is a key parameter for evaluating the transition speed of a logic device. A high I_{on} is advantageous for efficient applications such as high-performance servers with high switching velocity. One can calculate I_{on} (HP) and I_{on} (LP) by applying $V_g(\text{on/HP}) = V_g(\text{off/HP}) \pm V_{dd}$ and $V_g(\text{on/LP}) = V_g(\text{off/LP}) \pm V_{dd}$, respectively. In order to obtain the value of the on-state current the first step is making these DG ML MoSi₂N₄ MOSFETs reach the off-state current. Following the requirements of ITRS for the off-state current, the I_{off} of HP and LP devices were set to 0.1 and $5 \times 10^{-5} \mu\text{A}/\mu\text{m}$, respectively.

The calculated transfer characteristics of sub-5 nm gate-length MoSi₂N₄ MOSFETs are shown in Figs. 2(b)-2(g). As shown in Figs. 2(b)-2(g), all of the

MOSFETs have small enough source-drain leakage current to reach the off-state requirements for high-performance standards. This is own to the large band gap and simple energy band state in the conductive region. However, for the low-power application with $L_{UL} < 2$ nm, the 1 nm gate-length device cannot reach the requirement of the off-state current due to the short channel effect. The introduction of the underlap region enlarges the effective channel length and improves the MOSFETs' ability in reaching the off-state current, especially for the device with gate length $L_g = 1$ nm. Whereas, when the gate length is long enough, increasing UL has little effect on the device performance. This is because that the introduction of UL will inhibit the tunneling of carriers in the off state, especially for the devices with the short gate which had the relatively large tunneling effect. For the devices with long gate, the tunneling current was small, as well as the impact of UL. These phenomena can be noticeably observed by comparing Figs. 2(b) and 2(d), where the I - V curve for the 5 nm gate length device with different L_{UL} are almost overlapped in Fig. 2(d). We additionally explored the effect of increasing doping concentration on the MOSFETs current, i.e., with $5.0 \times 10^{13} \text{ cm}^{-2}$ electron doping on the electrodes for the device of $L_{UL} = 4$ nm. Compared with low doping-concentration case, the increase of doping concentration obviously increases the current under the same V_g .

We further summarized the values of I_{on} for the sub-5 nm MOSFETs, as shown in Fig. 3. It is seen that I_{on} generally monotonically increases with the gate length increasing. For the HP ML MoSi_2N_4 devices [Figs. 3(a) and 3(b)], the on-state current of high doping concentration case ($5.0 \times 10^{13} \text{ cm}^{-2}$) is much higher than that of low

doping concentration ($1.0 \times 10^{13} \text{ cm}^{-2}$). It is seen that only the n-type MOSFET with high concentration can meet the ITRS HP requirement ($900 \mu\text{A}/\mu\text{m}$), reaching up to 1206 and $1390 \mu\text{A}/\mu\text{m}$ for the 3 and 5 nm gate-length, respectively. Nevertheless, the highest I_{on} of the low doping concentration case reaches $817 \mu\text{A}/\mu\text{m}$, fulfilling 91% of the ITRS standard [Fig. 3(a)]. As for the p-type MOSFETs with low concentration, the highest I_{on} appears for a 3 nm gate-length MOSFET with $L_{\text{UL}} = 4\text{nm}$ [Fig. 3(b)]. Similar to the n-type MOSFETs, the I_{on} increases with the doping concentration increasing, where the p-type 5 nm gate-length MOSFET could get an $I_{\text{on}} \approx 618 \mu\text{A}/\mu\text{m}$ with doping concentration of $5.0 \times 10^{13} \text{ cm}^{-2}$. This value fulfills 69% of the ITRS standard. Note that the introduction of the underlap region can help to increase the I_{on} for the HP ML MoSi₂N₄ devices in most cases.

As for the LP application, the I_{on} of the n-type and p-type of the ML MoSi₂N₄ devices increases with the gate-length increasing from 1 to 3 nm, both of which can meet the ITRS HP standard ($295 \mu\text{A}/\mu\text{m}$) under certain L_{UL} [Figs. 3(c) and 3(d)]. The largest I_{on} of the n-type MOSFETs are 793 and $1025 \mu\text{A}/\mu\text{m}$ for the low doping concentration and the high doping concentration, respectively. The I_{on} of n-type MOSFETs can satisfy the ITRS LP standard requirement even as the gate-length goes down to 1 nm with $L_{\text{UL}} = 4 \text{ nm}$ ($315 \mu\text{A}/\mu\text{m}$) [Fig. 3(c)]. As for the p-type device, the minimum gate-length to fulfill the LP requirement is 3nm [Fig. 3(d)], where the largest I_{on} ($348 \mu\text{A}/\mu\text{m}$) appears with 5 nm gate-length and $L_{\text{UL}} = 1 \text{ nm}$.

It is noticed that the increase of underlap does not always improve the on-state current of the device [as indicated in Figs. 3(c) and 3(d)]. This feature can be owing to

two competing mechanisms: on one hand, the increase of underlap region makes the channel barrier longer, which decreases the transmission possibility and suppresses the short-channel effect (positive effect). On the other hand, the gate controlling capability of the underlap region becomes weaker with its length increasing, which would degrade the performance of the device (negative effect). These two conflicting effects imply that the length of the underlap should be optimized to obtain the highest on-state current.

To illustrate the function of underlap and modulation mechanism of gate more clearly, we have calculated the local density of state (LDOS) and transmission spectra of the 1 nm gate ML MoSi₂N₄ MOSFETs with different L_{UL} [Fig. 4] for the HP case. Here we defined the maximum electron barrier height Φ_m as the energy barrier to transport from the source to the drain. As shown in Figs. 4(a)-4(c), the same off-state current of $0.1\mu\text{A}/\mu\text{m}$, Φ_m is reduced from 0.26 eV at $L_{UL} = 0$ nm to 0.19 and 0.17 eV at $L_{UL} = 2$ and 4 nm, respectively. The calculated transmission spectra confirm the variation of transmission barrier [Fig. 4(d)]. When a voltage of 0.64 V is applied, the CBM of the ML MoSi₂N₄ in the channel region would move downward, leading to the on-state of the MOSFETs [Figs. 4(e)-4(g)]. From Fig. 3(a), I_{on} with $L_{UL} = 4$ nm is the highest, followed by the case with $L_{UL} = 2$ nm, and I_{on} in the one without UL is the lowest. This is because CBM becomes lower with the L_{UL} increasing, which leads to a higher on-state current. Correspondingly, the on-state transmission spectra edge at $L_{UL} = 4$ nm is the upmost within the bias window, which is consistent with the result of highest on-state current for $L_{UL} = 4$ nm. [Fig. 4(h)]. [The variation of the UL lead to](#)

different carrier barrier height Φ_m and barrier length, resulting in the difference of gate control.

C. Gate control

The ability of gate control of the FET in the subthreshold region is usually described by subthreshold swing (SS), which impacts on the device performance and decides the operating voltage of the device. The definition of the SS is

$$SS = \frac{\partial V_g}{\partial(\lg I_{DS})} \quad (2)$$

where I_{DS} is the drain current. Note that the smaller SS corresponds to the better gate control ability. Fig. 5 shows the calculated SS with different gate length (L_g) and underlap (L_{UL}). It is found that SS generally increases with the decreasing of the L_g and L_{UL} . In addition, for the n-type device without underlap ($L_{UL}=0$), the SS value sharply increases from 57 to 166 mV/dec with L_g downsizing from 5 to 1 nm. This feature shows that the underlap is beneficial to the reduce of SS. This is because that the devices with long L_{UL} can reach the off-state current with smaller V_g , which lead to the larger slope in the I - V_g figure. Such effect is more noticeable in the relatively short gate-length devices. For example, in the n-type case with $L_{UL} = 4$ nm, the SS of $L_g = 1$ nm MOSFETs can be reduced by 55% (from 166 to 75 mV/dec), while it can be only reduced by 23% (from 57 to 44 mV/dec) for $L_g = 5$ nm. The similar phenomenon is also observed in the p-type case. It is noticed that the minimum SS of the n-type and p-type MoSi₂N₄ MOSFETs are 44 and 58 mV/dec, respectively. Both of them are smaller than the Boltzmann's tyranny (60 mV/dec) that is believed to be fundamental limit of SS in MOSFETs at room temperature. [22] This limit is suitable

for classical transistors with long channel whose current is mainly composed of thermionic injection. In the MOSFETs with an ultrashort channel down to a few nanometers, the contribution of the tunneling current could help to make the value of SS fall below the Boltzmann's tyranny. Taking both the tunneling and thermionic currents into consideration, namely $I_{DS} = I_{tunnel} + I_{therm}$, the SS can be expressed as follows: [22]

$$SS = \frac{\partial V_g}{\partial(\lg I_{DS})} = \left[\frac{r_{tunnel}}{SS_{tunnel}} + \frac{1-r_{tunnel}}{SS_{therm}} \right]^{-1} \quad (3)$$

where

$$r_{tunnel} = \frac{I_{tunnel}}{I_{DS}}, \quad SS_{tunnel} = \frac{\partial V_g}{\partial(\lg I_{tunnel})}, \quad SS_{therm} = \frac{\partial V_g}{\partial(\lg I_{therm})}$$

In the transistors with long channel, the I_{tunnel} can be neglected, leading to $r_{tunnel} = 0$, $SS = SS_{therm}$, which has a fundamental limit of 60 mV/dec. In the transistors with ultrashort channel, the tunneling should be considered, the $r_{tunnel} \neq 0$, the SS can be below the Boltzmann's tyranny when the SS_{tunnel} is small enough. The tunneling current is presented as $I_{tunnel} = e^{-w\sqrt{m^*\Phi_B}}$, where Φ_B is the average barrier height, and w is the width of the barrier. According to the LDOS maps, the Φ_B decrease rapidly with the change of V_g , leading to a great change of I_{tunnel} . Thus, the SS_{tunnel} can be very small, which could help to make the value of SS below the limit of 60 mV/dec.

D. Delay time and power consumption

We have additionally explored the property of switching speed in the MoSi₂N₄ MOSFETs, which is an essential figure of merit for a digital circuit. The switching speed can be characterized directly by the intrinsic delay time (τ), as

$$\tau = \frac{C_g V_{dd}}{I_{on}} \quad (4)$$

where C_g is total gate capacitance, defined as the sum of the channel capacitance (C_{ch}) and the gate fringing capacitance (C_f) per width. The C_f is speculated to be two times of the intrinsic channel capacitance, and C_{ch} can be calculated by the formula

$$C_{ch} = \frac{\partial Q_{ch}}{W \partial V_g} \quad (5)$$

with Q_{ch} being the total charge in the central region and W being the channel width, respectively. The calculated values of C_g for the n- and p-type sub-5 nm ML MoSi₂N₄ MOSFETs in Tables SI and SII [within the Supplemental Material [51]], respectively. It is found that C_g (0.099–0.14 for n-type, 0.102–0.149 fF/μm for p-type) of the MoSi₂N₄ MOSFETs is much smaller than either the HP (0.6 fF/μm) or LP (0.69 fF/μm) ITRS standard, respectively. Figs. 6(a) and 6(b) further show the values of τ for n- and p-type sub-5 nm MoSi₂N₄ devices as a function of L_g . It is shown that the intrinsic delay time τ of both the n- and p-type devices with various gate-length and L_{UL} can fulfill the ITRS requirement (0.423 ps) for the HP devices. Also, all the intrinsic delay time τ can meet the ITRS LP standard (1.493 ps) for the LP devices, except for the one in n-type with $L_g = 1$ nm and $L_{UL} = 2$ nm due to the very low I_{on} (44 μA/μm). Moreover, the value of τ under certain L_g and L_{UL} can be several (ten) times smaller than the HP (LP) ITRS standard, indicating the great potential applications in high switching speed of MoSi₂N₄ MOSFETs.

Another significant concern for FET applications is the switching energy cost by power delay product (PDP) which can be calculated by the formula

$$PDP = V_{dd} I_{on} \tau = C_g V_{dd}^2 \quad (6)$$

Figs 6(c) and 6(d) show the calculated PDP of n-type and p-type sub-5 nm MoSi₂N₄ devices as functions of L_g , respectively. In both cases, PDP monotonously decreases with increase of L_{UL} . In addition, PDP of both n-type (0.023–0.101 fJ/ μ m) and p-type (0.026–0.121 fJ/ μ m) sub-5 nm MOSFETs are much lower than the ITRS requirements for HP (0.24 fJ/ μ m) and LP (0.28 fJ/ μ m) standards. This feature verifies that the MoSi₂N₄ MOSFETs devices also have advantage of low-power consumption.

E. Discussion

The comparison of the main parameters including on-state current, subthreshold swing, delay time and power-delay product of ML MoSi₂N₄ MOSFETs and other 2D MOSFETs with $L_g \leq 5$ nm based on *ab initio* quantum transport calculations for HP and LP devices is shown in Table I and II, respectively. There are some 2D MOSFETs with very high on-state current for HP application, such as Phosphorene (4500 μ A/ μ m), BiH (2320 μ A/ μ m), Tellurene (2114 μ A/ μ m) and Arsenene (2030 μ A/ μ m). However, they are all p-type MOSFETs and are not suitable for n-type doped, which hinders the application in Complementary Metal Oxide Semiconductor (CMOS). For the n-type MOSFETs, the performance of ML MoSi₂N₄ is better than other 2D materials, especially for the LP application.

Two-dimensional MoS₂ transistors have been extensively studied for many years, both in experimental and simulation ways. The electronic structures of MoS₂ and MoSi₂N₄ are very similar. However, the performance of ML MoSi₂N₄ transistor is much better than that of ML MoS₂ transistor. the current along the transport direction is defined as $I = Nev$, where N is the number of carriers and v is the velocity of

carriers and is defined as $v = \mu E$, where μ and E are the carrier mobility and electric field, respectively. The on-state current is proportional to the carrier mobility. For 2D materials, the intrinsic carrier mobility can be calculated using the following equation:

$$\mu_{2D} = \frac{2e\hbar^3 C}{3k_B T |m^*|^2 E_1^2} \quad (7)$$

where C is the elastic modulus, m^* is the effective mass, T is the temperature and E_1 is the deformation potential (DP) constant. The elastic modulus of ML MoSi₂N₄ is about 4 times high than that of MoS₂ (about 530 N/m for MoSi₂N₄ and 128 N/m for MoS₂, both for holes and electrons), which makes the higher carrier mobility of the monolayer MoSi₂N₄ (about 1227 cm² V⁻¹ s⁻¹ for holes and 288 cm² V⁻¹ s⁻¹ for electrons) than that of MoS₂ (about 200 cm² V⁻¹ s⁻¹ for holes and 152 cm² V⁻¹ s⁻¹ for electrons). [34] Therefore, the ML MoSi₂N₄ transistors have much higher on-state current than that of ML MoS₂.

TABLE I. Comparison of the upper performance limit of the ML MoSi₂N₄ MOSFETs with other 2D MOSFETs with $L_g \leq 5$ nm for HP devices.

	Doping type	$I_{ON}(\mu A/\mu m)$	SS(mV/dec)	τ (ps)	PDP(fJ/ μm)
MoS ₂ [53]	n-type	473	58	1.287	0.195
	p-type	440	46	0.396	0.096
WSe ₂ [54]	p-type	1464	82	0.168	0.156
Bi ₂ O ₂ Se [33]	n-type	916	114	0.240	0.141
	p-type	585	96	0.375	0.140
BiH [55]	p-type	2320	77	0.020	0.029
GeSe [52]	n-type	518	130	0.124	0.041
	p-type	1703	60	0.054	0.059
Phosphorene [22]	p-type	4500	76	0.055	0.135
Tellurene [29]	p-type	2114	102	0.068	0.098
Silicane [56]	n-type	1374	65	0.042	0.037
	p-type	871	67	0.075	0.043
Arsenene [57]	p-type	2030	77	0.017	0.032

MoSi ₂ N ₄	n-type	1390	44	0.064	0.057
	p-type	618	64	0.140	0.055

TABLE II. Comparison of the upper performance limit of the ML MoSi₂N₄ MOSFETs with other 2D MOSFETs with $L_g \leq 5$ nm for LP devices.

	Doping type	$I_{ON}(\mu A/\mu m)$	SS(mV/dec)	τ (ps)	PDP(fJ/ μm)
MoS ₂ [53]	n-type	324	56	0.552	0.093
	p-type	425	46	0.411	0.075
WSe ₂ [54]	p-type	1132	63	0.149	0.108
ReS ₂ [58]	p-type	329	72	0.700	0.150
BiH [55]	p-type	179	67	0.168	0.018
GeSe [52]	n-type	274	90	0.320	0.055
Phosphorene [22]	p-type	857	85	0.193	0.108
Tellurene [29]	p-type	451	57	0.206	0.063
Silicane [56]	n-type	467	77	0.054	0.016
	p-type	378	67	0.136	0.012
Arsenene [57]	p-type	341	77	0.101	0.023
MoSi ₂ N ₄	n-type	1025	44	0.086	0.057
	p-type	355	70	0.265	0.060

IV. CONCLUSION

To summarize, we have explored the performance limit of sub-5 nm n- and p-type ML MoSi₂N₄ MOSFETs by applying precise *ab initio* quantum transport simulations. We have found that the middle MoN₂ layer of MoSi₂N₄ is responsible for the electron transmission, and the variation of on-state current in the MoSi₂N₄ MOSFETs can be effectively manipulated by the length of gate and underlap, as well as the doping concentration. More importantly, a competing mechanism for the influence of underlap length on the on-state current has also been found, indicating there is an optimized on-state current for a certain assemble of gate length and underlap length. In addition, we have also found that the n-type devices the optimized

on-state current can reach 1390 and 1025 $\mu\text{A}/\mu\text{m}$ for the HP and LP applications, respectively, both of which satisfy the ITRS requirements. Whereas, the optimized on-state current can meet the LP application (348 $\mu\text{A}/\mu\text{m}$) for the p-type devices. Finally, we have found that the sub-5 nm MoSi_2N_4 MOSFETs can have unusually short intrinsic delay time and low power delay product compared with the standards of ITRS, which make the devices with high speed and low power consumption. Considering that MoSi_2N_4 is remarkably stable in air, its sub-5 nm MOSFETs devices with high-performance are expected to be widely realized in the near future.

Acknowledgements

“J. S. H and P. L contributed equally to this work. We are grateful for useful discussions with Prof. Ying Guo. This work was supported by the National Key R&D Program of China (2018YFB0407600), National Natural Science Foundation of China (No. 12074301 and No. 12004295), Fundamental Research Funds for Central Universities (No. xzy012019062), and Open Research Fund of Key Laboratory of Polar Materials and Devices, Ministry of Education. P. L. also thanks China’s Postdoctoral Science Foundation funded project (No.2020M673364).

References

- [1] S. Salahuddin, K. Ni, and S. Datta, The Era of Hyper-Scaling in Electronics, *Nat. Electron.* **1**, 442 (2018).
- [2] N. G. Orji, M. Badaroglu, B. M. Barnes, C. Beitia, B. D. Bunday, U. Celano, R. J. Kline, M. Neisser, Y. Obeng, and A. E. Vladar, Metrology for the next Generation of Semiconductor Devices, *Nat. Electron.* **1**, 532 (2018).
- [3] R. Chau, B. Doyle, S. Datta, J. Kavalieros, and K. Zhang, Integrated Nanoelectronics for the Future, *Nat. Mater.* **6**, 810 (2007).
- [4] T. N. Theis and P. M. Solomon, It ’ s Time to Reinvent the Transistor ! An Emergent Change

- Of, Science 1600 (2010).
- [5] Y. Liu, X. Duan, Y. Huang, and X. Duan, Two-Dimensional Transistors beyond Graphene and TMDCs, *Chem. Soc. Rev.* **47**, 6388 (2018).
- [6] D. Akinwande, C. Huyghebaert, C. H. Wang, M. I. Serna, S. Goossens, L. J. Li, H. S. P. Wong, and F. H. L. Koppens, Graphene and Two-Dimensional Materials for Silicon Technology, *Nature* **573**, 507 (2019).
- [7] Z. Ni, M. Ye, J. Ma, Y. Wang, R. Quhe, J. Zheng, L. Dai, D. Yu, J. Shi, J. Yang, S. Watanabe, and J. Lu, Performance Upper Limit of Sub-10 Nm Monolayer MoS₂ Transistors, *Adv. Electron. Mater.* **2**, 1600191 (2016).
- [8] M. Zeng, Y. Xiao, J. Liu, K. Yang, and L. Fu, Exploring Two-Dimensional Materials toward the Next-Generation Circuits: From Monomer Design to Assembly Control, *Chem. Rev.* **118**, 6236 (2018).
- [9] K. Majumdar, C. Hobbs, and P. D. Kirsch, Benchmarking Transition Metal Dichalcogenide MOSFET in the Ultimate Physical Scaling Limit, *IEEE Electron Device Lett.* **35**, 402 (2014).
- [10] S. Zhang, S. Guo, Z. Chen, Y. Wang, H. Gao, J. Gómez-Herrero, P. Ares, F. Zamora, Z. Zhu, and H. Zeng, Recent Progress in 2D Group-VA Semiconductors: From Theory to Experiment, *Chem. Soc. Rev.* **47**, 982 (2018).
- [11] F. Schwierz, Graphene Transistors, *Nat. Nanotechnol.* **5**, 487 (2010).
- [12] G. Fiori, A. Betti, S. Bruzzone, and G. Iannaccone, Lateral Graphene-HBCN Heterostructures as a Platform for Fully Two-Dimensional Transistors, *ACS Nano* **6**, 2642 (2012).
- [13] W. Zhou, J. Chen, P. Bai, S. Guo, S. Zhang, X. Song, L. Tao, and H. Zeng, Two-Dimensional Pnictogen for Field-Effect Transistors, *Research* **2019**, 1 (2019).
- [14] A. Allain, J. Kang, K. Banerjee, and A. Kis, Electrical Contacts to Two-Dimensional Semiconductors, *Nat. Mater.* **14**, 1195 (2015).
- [15] S. B. Desai, S. R. Madhupathy, A. B. Sachid, J. P. Llinas, Q. Wang, G. H. Ahn, G. Pitner, M. J. Kim, J. Bokor, C. Hu, H. S. P. Wong, and A. Javey, MoS₂ Transistors with 1-Nanometer Gate Lengths, *Science* **354**, 99 (2016).
- [16] L. Xie, M. Liao, S. Wang, H. Yu, L. Du, J. Tang, J. Zhao, J. Zhang, P. Chen, X. Lu, G. Wang, G. Xie, R. Yang, D. Shi, and G. Zhang, Graphene-Contacted Ultrashort Channel Monolayer MoS₂ Transistors, *Adv. Mater.* **29**, 1702522 (2017).
- [17] K. Xu, D. Chen, F. Yang, Z. Wang, L. Yin, F. Wang, R. Cheng, K. Liu, J. Xiong, Q. Liu, and J. He, Sub-10 Nm Nanopattern Architecture for 2D Material Field-Effect Transistors, *Nano Lett.* **17**, 1065 (2017).
- [18] A. Nourbakhsh, A. Zubair, R. N. Sajjad, T. K. G. Amir, W. Chen, S. Fang, X. Ling, J. Kong, M. S. Dresselhaus, E. Kaxiras, K. K. Berggren, D. Antoniadis, and T. Palacios, MoS₂ Field-Effect Transistor with Sub-10 Nm Channel Length, *Nano Lett.* **16**, 7798 (2016).
- [19] M. Fang, F. Wang, Y. Han, Y. Feng, T. Ren, Y. Li, D. Tang, Z. Song, and K. Zhang, Controlled Growth of Bilayer-MoS₂ Films and MoS₂-Based Field-Effect Transistor (FET) Performance Optimization, *Adv. Electron. Mater.* **4**, 1700524 (2018).
- [20] International Technology Roadmap for Semiconductors (ITRS), <http://www.itrs2.net/>, 2013.
- [21] P. H. Ho, Y. R. Chang, Y. C. Chu, M. K. Li, C. A. Tsai, W. H. Wang, C. H. Ho, C. W. Chen, and P. W. Chiu, High-Mobility InSe Transistors: The Role of Surface Oxides, *ACS Nano* **11**, 7362 (2017).
- [22] R. Quhe, Q. Li, Q. Zhang, Y. Wang, H. Zhang, J. Li, X. Zhang, D. Chen, K. Liu, Y. Ye, L. Dai,

- F. Pan, M. Lei, and J. Lu, Simulations of Quantum Transport in Sub-5-Nm Monolayer Phosphorene Transistors, *Phys. Rev. Appl.* **10**, 024022 (2018).
- [23] J. D. Wood, S. A. Wells, D. Jariwala, K. S. Chen, E. Cho, V. K. Sangwan, X. Liu, L. J. Lauhon, T. J. Marks, and M. C. Hersam, Effective Passivation of Exfoliated Black Phosphorus Transistors against Ambient Degradation, *Nano Lett.* **14**, 6964 (2014).
- [24] W. Zhou, S. Zhang, Y. Wang, S. Guo, H. Qu, P. Bai, Z. Li, and H. Zeng, Anisotropic In-Plane Ballistic Transport in Monolayer Black Arsenic-Phosphorus FETs, *Adv. Electron. Mater.* **6**, 1901281 (2020).
- [25] W. Zhou, S. Zhang, S. Guo, Y. Wang, J. Lu, X. Ming, Z. Li, H. Qu, and H. Zeng, Designing Sub-10-Nm Metal-Oxide-Semiconductor Field-Effect Transistors via Ballistic Transport and Disparate Effective Mass: The Case of Two-Dimensional Bi N, *Phys. Rev. Appl.* **13**, 044066 (2020).
- [26] J. Zhao, H. Liu, Z. Yu, R. Quhe, S. Zhou, Y. Wang, C. C. Liu, H. Zhong, N. Han, J. Lu, Y. Yao, and K. Wu, Rise of Silicene: A Competitive 2D Material, *Prog. Mater. Sci.* **83**, 24 (2016).
- [27] S. Zhang, M. Xie, F. Li, Z. Yan, Y. Li, E. Kan, W. Liu, Z. Chen, and H. Zeng, Semiconducting Group 15 Monolayers: A Broad Range of Band Gaps and High Carrier Mobilities, *Angew. Chemie* **128**, 1698 (2016).
- [28] E. Zhang, Y. Jin, X. Yuan, W. Wang, C. Zhang, L. Tang, S. Liu, P. Zhou, W. Hu, and F. Xiu, ReS₂-Based Field-Effect Transistors and Photodetectors, *Adv. Funct. Mater.* **25**, 4076 (2015).
- [29] J. Yan, H. Pang, L. Xu, J. Yang, R. Quhe, X. Zhang, Y. Pan, B. Shi, S. Liu, L. Xu, J. Yang, F. Pan, Z. Zhang, and J. Lu, Excellent Device Performance of Sub-5-Nm Monolayer Tellurene Transistors, *Adv. Electron. Mater.* **5**, 1900226 (2019).
- [30] L. Tao, E. Cinquanta, D. Chiappe, C. Grazianetti, M. Fanciulli, M. Dubey, A. Molle, and D. Akinwande, Silicene Field-Effect Transistors Operating at Room Temperature, *Nat. Nanotechnol.* **10**, 227 (2015).
- [31] L. Li, Y. Yu, G. J. Ye, Q. Ge, X. Ou, H. Wu, D. Feng, X. H. Chen, and Y. Zhang, Black Phosphorus Field-Effect Transistors, *Nat. Nanotechnol.* **9**, 372 (2014).
- [32] S. Guo, Y. Zhang, Y. Ge, S. Zhang, H. Zeng, and H. Zhang, 2D V-V Binary Materials: Status and Challenges, *Adv. Mater.* **31**, 1902352 (2019).
- [33] J. Yang, R. Quhe, Q. Li, S. Liu, L. Xu, Y. Pan, H. Zhang, X. Zhang, J. Li, J. Yan, B. Shi, H. Pang, L. Xu, Z. Zhang, J. Lu, and J. Yang, Sub 10 Nm Bilayer Bi₂O₂Se Transistors, *Adv. Electron. Mater.* **5**, 1800720 (2019).
- [34] Y.-L. Hong, Z. Liu, L. Wang, T. Zhou, W. Ma, C. Xu, S. Feng, L. Chen, M.-L. Chen, D.-M. Sun, X.-Q. Chen, H.-M. Cheng, and W. Ren, Chemical Vapor Deposition of Layered Two-Dimensional MoSi₂N₄ Materials, *Science* **369**, 670 (2020).
- [35] Q. Wu, L. Cao, Y. S. Ang, and L. K. Ang, Semiconductor-to-Metal Transition in Bilayer MoSi₂N₄ and WSi₂N₄ with Strain and Electric Field, *Appl. Phys. Lett.* **118**, 113102 (2021).
- [36] S. D. Guo, Y. T. Zhu, W. Q. Mu, and W. C. Ren, Intrinsic Piezoelectricity in Monolayer MSi₂N₄ (M = Mo, W, Cr, Ti, Zr and Hf), *Epl* **132**, 57002 (2020).
- [37] H. Zhong, W. Xiong, P. Lv, J. Yu, and S. Yuan, Strain-Induced Semiconductor to Metal Transition in MA₂Z₄ Bilayers (M = Ti, Cr, Mo; A = Si; Z = N, P), *Phys. Rev. B* **103**, 085124 (2021).
- [38] Q. Wang, L. Cao, S.-J. Liang, W. Wu, G. Wang, C. H. Lee, W. L. Ong, H. Y. Yang, L. K. Ang,

- S. A. Yang, and Y. S. Ang, Efficient Ohmic Contacts and Built-in Atomic Sublayer Protection in MoSi₂N₄ and WSi₂N₄ Monolayers, *Npj 2D Mater. Appl.* **5**, 71 (2021).
- [39] L. Cao, G. Zhou, Q. Wang, L. K. Ang, and Y. S. Ang, Two-Dimensional van Der Waals Electrical Contact to Monolayer MoSi₂N₄, *Appl. Phys. Lett.* **118**, 013106 (2021).
- [40] D. Joubert, From Ultrasoft Pseudopotentials to the Projector Augmented-Wave Method, *Phys. Rev. B - Condens. Matter Mater. Phys.* **59**, 1758 (1999).
- [41] G. Kresse and J. Hafner, Ab Initio Molecular Dynamics for Liquid Metals, *Phys. Rev. B* **47**, 558 (1993).
- [42] R. A. Vargas-Hernández, Bayesian Optimization for Calibrating and Selecting Hybrid-Density Functional Models, *J. Phys. Chem. A* **124**, 4053 (2020).
- [43] J. P. Perdew, K. Burke, and M. Ernzerhof, Generalized Gradient Approximation Made Simple, *Phys. Rev. Lett.* **77**, 3865 (1996).
- [44] H. J. Monkhorst and J. D. Pack, Special Points for Brillouin-Zone Integrations, *Phys. Rev. B* **13**, 5188 (1976).
- [45] M. Brandbyge, J. L. Mozos, P. Ordejón, J. Taylor, and K. Stokbro, Density-Functional Method for Nonequilibrium Electron Transport, *Phys. Rev. B - Condens. Matter Mater. Phys.* **65**, 1654011 (2002).
- [46] *QuantumATK Q-2019.12, Synopsys QuantumATK (<https://www.synopsys.com/silicon/quantumatk.html>).*
- [47] S. Datta and H. van Houten, Electronic Transport in Mesoscopic Systems, *Phys. Today* **49**, 70 (1996).
- [48] H. Zhong, R. Quhe, Y. Wang, Z. Ni, M. Ye, Z. Song, Y. Pan, J. Yang, L. Yang, M. Lei, J. Shi, and J. Lu, Interfacial Properties of Monolayer and Bilayer MoS₂ Contacts with Metals: Beyond the Energy Band Calculations, *Sci. Rep.* **6**, 21786 (2016).
- [49] Y. Wang, R. X. Yang, R. Quhe, H. Zhong, L. Cong, M. Ye, Z. Ni, Z. Song, J. Yang, J. Shi, J. Li, and J. Lu, Does P-Type Ohmic Contact Exist in WSe₂-Metal Interfaces?, *Nanoscale* **8**, 1179 (2016).
- [50] A. H. D. Cheng and D. T. Cheng, Heritage and Early History of the Boundary Element Method, *Eng. Anal. Bound. Elem.* **29**, 268 (2005).
- [51] See Supplemental Material at [URL will be inserted by publisher] for the specific data on the transport properties of FETs and the band structure of monolayer MoSi₂N₄.
- [52] Y. Guo, F. Pan, G. Zhao, Y. Ren, B. Yao, H. Li, and J. Lu, Sub-5 nm Monolayer Germanium Selenide (GeSe) MOSFETs: Towards a High Performance and Stable Device, *Nanoscale* **12**, 15443 (2020).
- [53] H. Zhang, B. Shi, L. Xu, J. Yan, W. Zhao, Z. Zhang, Z. Zhang, and J. Lu, Sub-5 nm Monolayer MoS₂ Transistors toward Low-Power Devices, *ACS Appl. Electron. Mater.* **3**, 1560 (2021).
- [54] X. Sun, L. Xu, Y. Zhang, W. Wang, S. Liu, C. Yang, Z. Zhang, and J. Lu, Performance Limit of Monolayer WSe₂ Transistors; Significantly Outperform Their MoS₂ Counterpart, *ACS Appl. Mater. Interfaces* **12**, 20633 (2020).
- [55] M. Ye, S. Liu, H. Zhang, B. Shi, J. Li, X. Zhang, J. Yan, and J. Lu, Sub-5 nm Monolayer BiH Transistors, *ACS Appl. Electron. Mater.* **1**, 2103 (2019).
- [56] Y. Pan, J. Dai, L. Xu, J. Yang, X. Zhang, J. Yan, J. Li, B. Shi, S. Liu, H. Hu, M. Wu, and J. Lu, Sub-5-nm Monolayer Silicene Transistor: A First-Principles Quantum Transport Simulation, *Phys. Rev. Appl.* **14**, 024016 (2020).

- [57] Y. Wang, P. Huang, M. Ye, R. Quhe, Y. Pan, H. Zhang, H. Zhong, J. Shi, and J. Lu, Many-Body Effect, Carrier Mobility, and Device Performance of Hexagonal Arsenene and Antimonene, *Chem. Mater.* **29**, 2191 (2017).
- [58] R. Quhe, J. Chen, and J. Lu, A Sub-10 nm Monolayer ReS₂ Transistor for Low-Power Applications, *J. Mater. Chem. C* **7**, 1604 (2019).

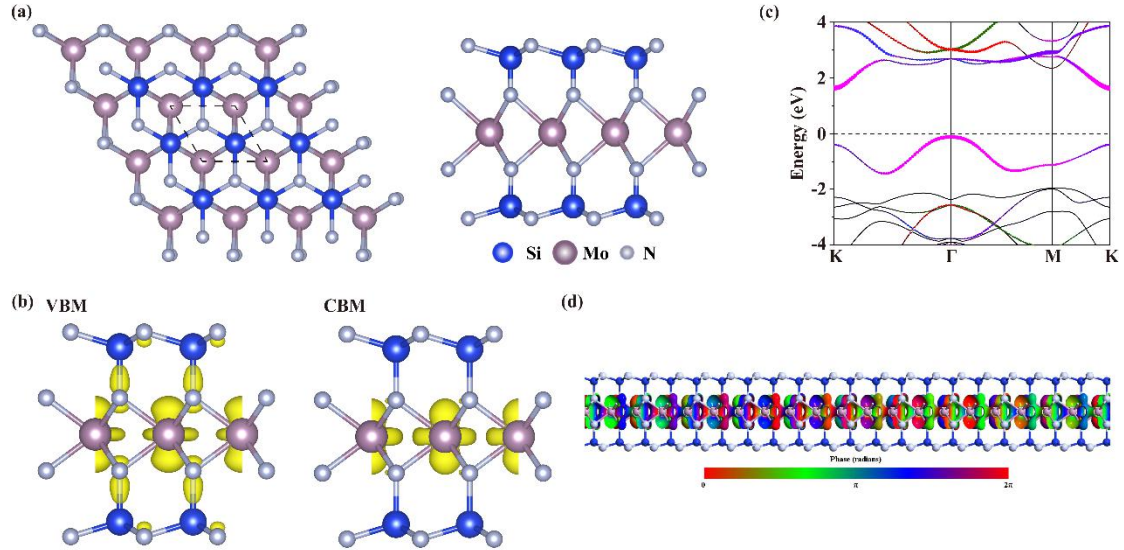


FIG. 1. (a) Top view and side view of ML MoSi₂N₄, dashed lines represent the primitive unit cell of ML MoSi₂N₄. Blue, purple and white balls represent silicon, molybdenum and nitrogen atoms, respectively. (b) Band-decomposed charge-density distributions corresponding to valence-band maximum (VBM) and conduction-band minimum (CBM) of ML MoSi₂N₄. The isovalue is 0.02 e/bohr³. (c) Electronic band structure of monolayer MoSi₂N₄. The different orbitals of Mo are mapped with different colors: Mo-d_{xy} orbital, blue; Mo-d_{yz} orbital, green; Mo -d_{xz} orbital, red; Mo-d_z² orbital, magenta; Mo-d_{x²-y²} orbital, purple and Mo-s orbital, orange. (d) Transmission eigenstates at K point (1/3,1/3) and E = 0.32 eV under onstate ($V_g = 0$ V). The isovalue is 0.2 au.

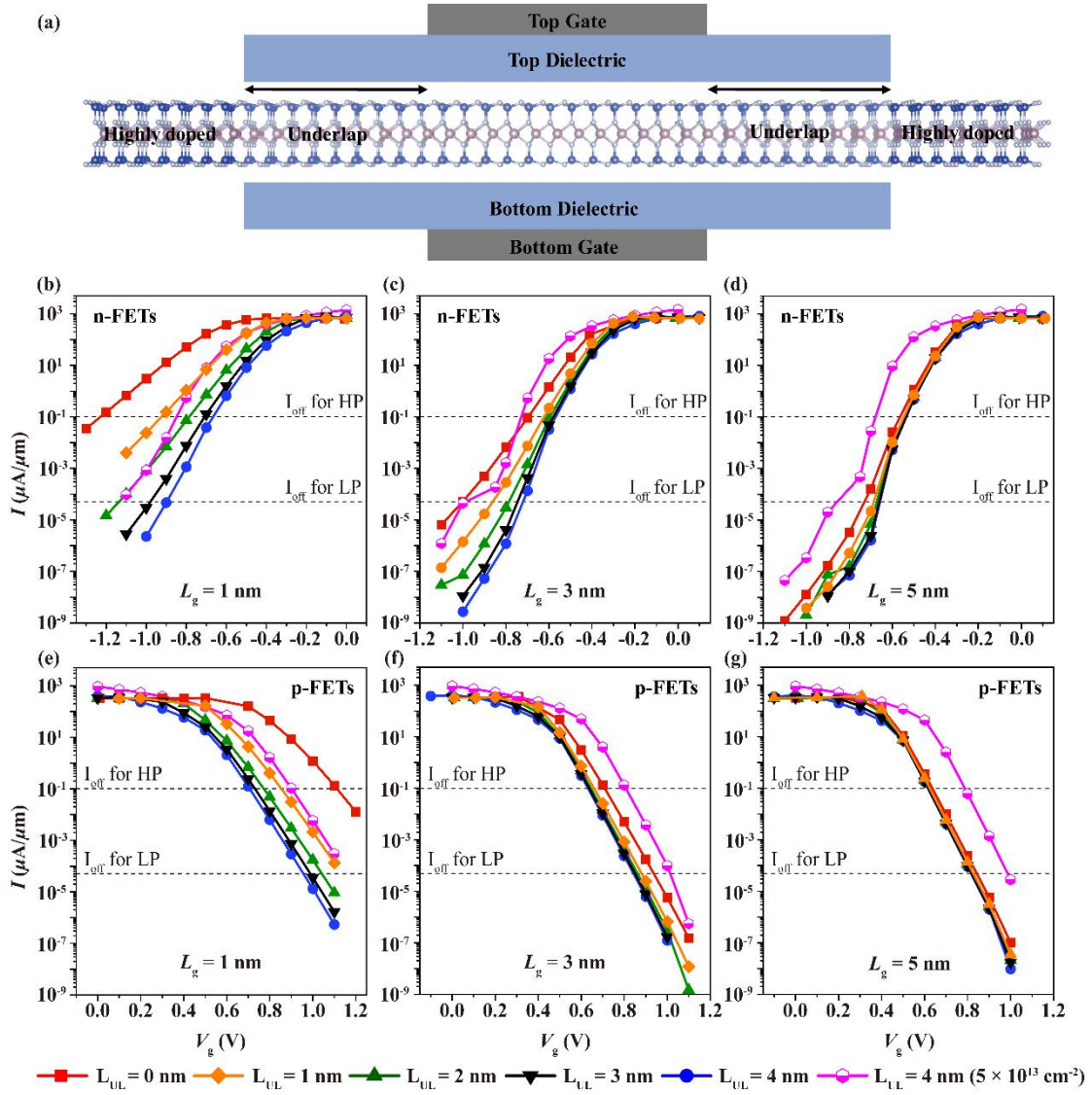


FIG. 2. (a) Schematic diagram of the DG ML MoSi₂N₄ MOSFETs. (b-g) I - V_g characteristics of n- and p-type FETs with different gate lengths and L_{UL} for $V_b = 0.64$ V.

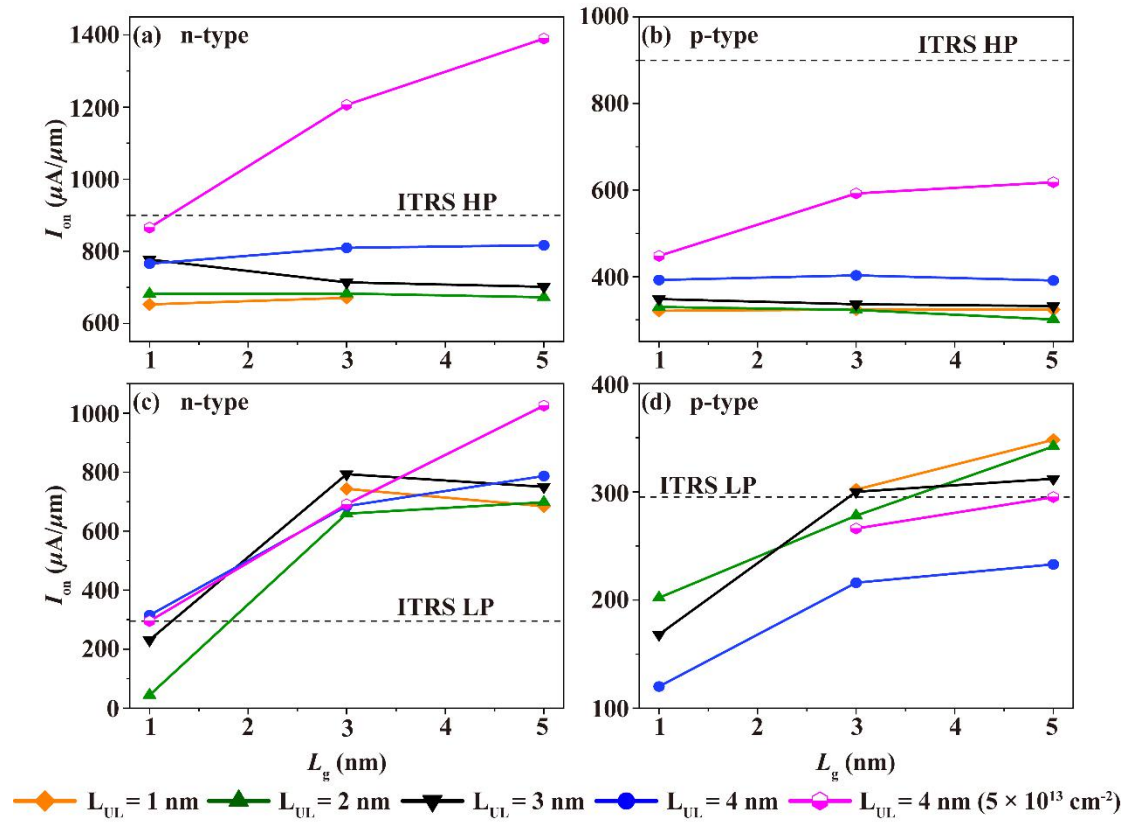


FIG. 3. On-state current as a function of the gate length for n- and p-type FETs with different L_{UL} . Black dashed lines represent the ITRS HP and LP requirements.

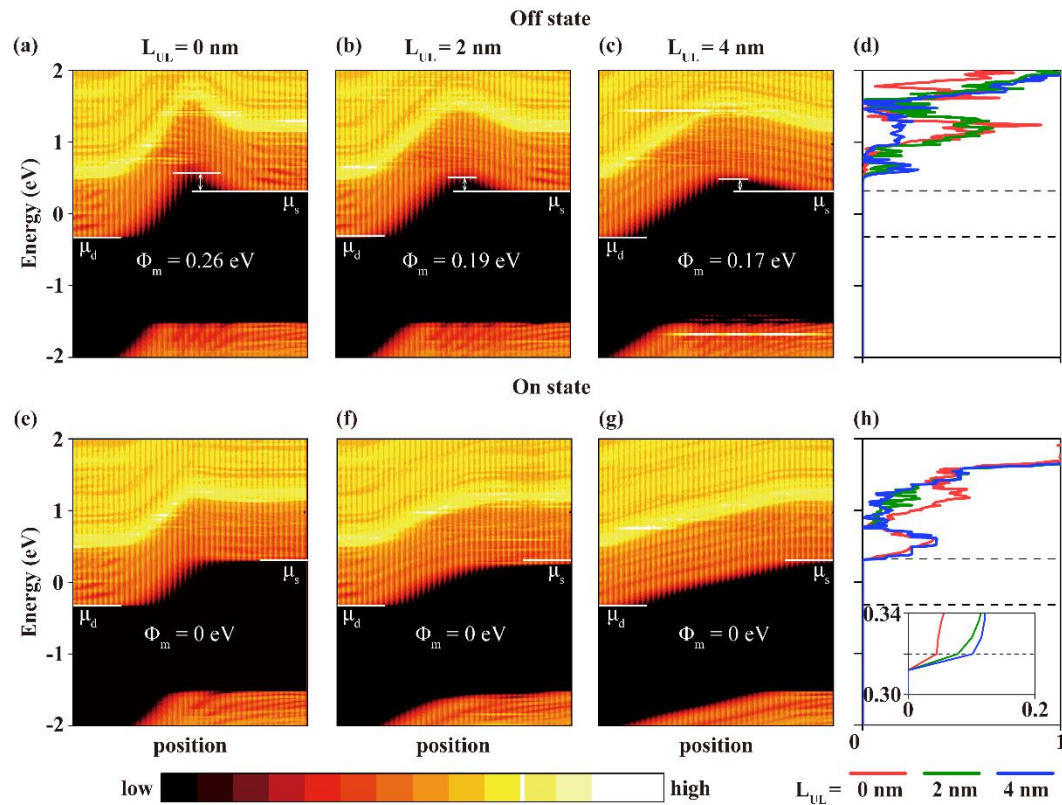


FIG. 4. Spatial resolved LDOS and transmission spectra for n-type FETs in the on and off states

with 1 nm gate length. Transmission spectra near the CBM of MoSi₂N₄ are shown in the inset in (h). μ_s and μ_d are the electrochemical potential of the source and drain, respectively.

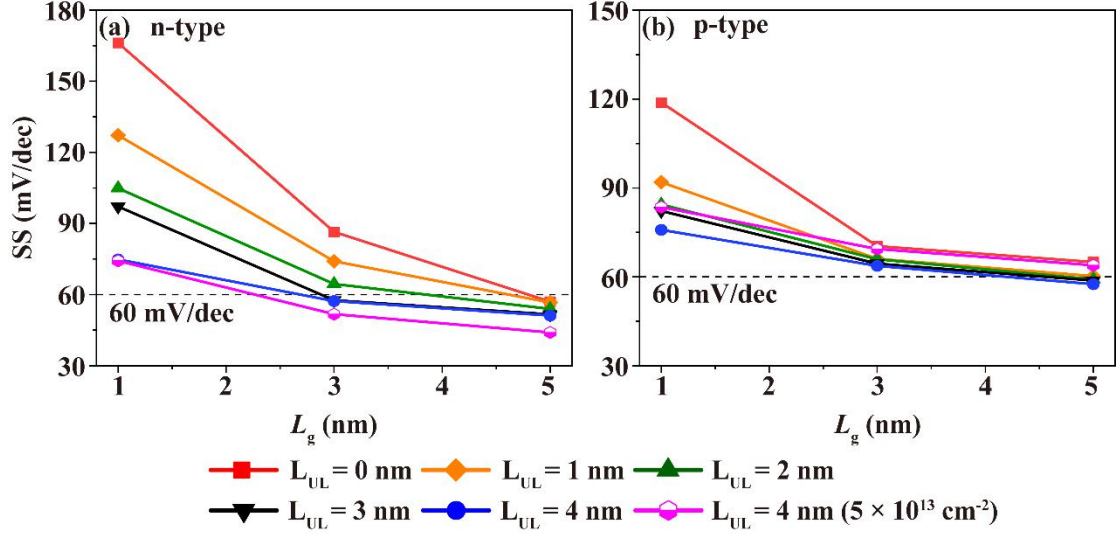


FIG. 5. Subthreshold swing (SS) as a function of gate length for n- and p-type FETs with different L_{UL} . Black dashed lines indicate the Boltzmann limit of 60 mV/dec for SS at room temperature.

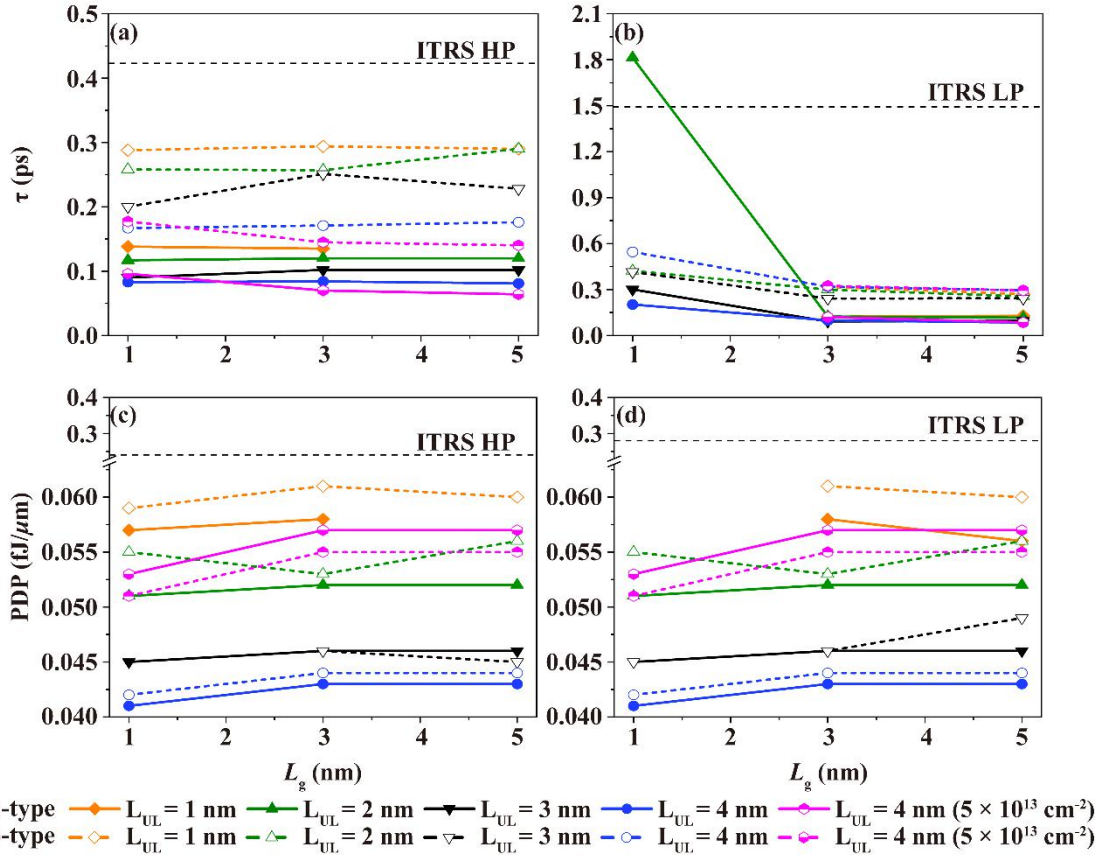


FIG. 6. Intrinsic delay time (τ) (a–b) and power-delay product (PDP) (c–d) as a function of gate length for n- and p-type FETs with different L_{UL} . Black dashed lines are the ITRS HP and LP requirements for τ and PDP, respectively.

